Detection and mapping of ghost-rock features in the Tournaisis area through geophysical methods – an overview

Olivier KAUFMANN & John DECEUSTER

University of Mons – Faculty of Engineering, Geology and Applied Geology Department, 20 Place du Parc, 7000 Mons (Belgium)

ABSTRACT In the context of cover-collapse sinkholes, as in the Tournaisis area, the detection of palaeokarst features allows to delineate, at a local scale, areas that might be subject to future collapse. These areas should therefore be avoided or dealt with in the perspective of earthworks for civil engineering. Before the last decade, karst mapping in this context was often wrongly considered as a cavity detection problem and tackled in this way. A better understanding of these phenomena allows developing more appropriate detection methods. We precise the geological settings and karst context of the Tournaisis. We present the key characteristics of the palaeokarsts and the main contrasts in petrophysical properties expected between alterite (ghost-rock) and bedrock. Given these contrasts and the wide range of overburden thicknesses found in the Tournaisis, we evidence the main advantages and major limitations of potentially effective geophysical investigation methods. We illustrate our purpose by describing some results of electrical resistivity tomography and seismic surveys applied to palaeokarst detection. These results are assessed using numerous geotechnical data and geological knowledge. Finally, we show how these results could be used for geological and geotechnical problem solving in particular trough the design of adapted detection and mapping strategies.

**KEYWORDS**: imaging, karst, ghost-rock, geophysics

1. Introduction

Detecting and mapping palaeokarst features that lie hidden under a soil or overburden is of importance in several cases, such as in karst aquifer vulnerability assessment, quarry works planning, karst risks mitigation. In the context of cover-collapse sinkholes, the detection of these features allows to delineate at a local scale areas that might be subject to future collapse and should be avoided or dealt with. In the perspective of earthworks for civil engineering works, such information may be of paramount importance at the planning stage to position the works or to select suitable and effective technical solutions. In the same way, in limestone quarry works, overburden removal, groundwater management strategy and operation planning might also benefit from a better knowledge of weathering spatial distribution and intensity.

At a regional scale, integrated methodologies have been developed to assess karst hazards (e.g., Edmonds et al., 1987, Kaufmann & Quinif, 2002, Benson et al., 2003, Waltham et al., 2005, Caramanna et al., 2008, Cooper, 2008, Galve et al. 2009) as well as to map karst groundwater intrinsic vulnerability: EPIK (Dörfliger et al., 1999), REKS (Malik & Svasta, 1999), PaPRIKA (Kavouri et al., 2011), RISKE (Pételet-Giraud et al., 2000), PI (Goldscheider, 2005), KARSTIC (Davis et al., 2002) and the COP and COP+K method (Andreo et al., 2009). Since more than ten years, a set of basic management maps called "karst constraints maps" (derived from a hazard susceptibility map, land-use planning maps and the regional regulations and recommendations to control development in karst areas) is available for land-use planning at a regional scale in the Walloon Region of Belgium (Van Dijck & Michel, 2006). These maps show sizeable areas of low to high karst hazard levels (Kaufmann & Quinif, 2002). . They are drawn at a regional scale while karst hazard is often highly variable in space at the local scale needed for building purposes (e.g., Deceuster et al., 2006, Kaufmann et al., 2012). The knowledge of local underground conditions has to be improved before the local authorities issue a building permit in karst areas. When the presence of karst features cannot be predicted from surface hints, as in most covered karst areas, specific methodologies are needed.

Geotechnical investigations like destructive boreholes or static cone penetration tests (CPTs) have shown some limitations to detect such targets. Indeed, the geometry of palaeokarst features is often complex and often exhibits vertical elongation. The depth of penetration of CPTs could be limited due to the presence of competent cover materials such as marls or chalks. Though these direct investigations are required to precise the nature of soils and estimate soil resistance, they give only punctual data. The number of drill holes needed to reliably map buried karst features or detect sinkholes rises quickly with the site dimension,

as well as the costs of such investigations. In practice the number of geotechnical tests is therefore limited and the reliability of interpretations based only on such investigations tends to be poor (Thomas & Roth, 1999).
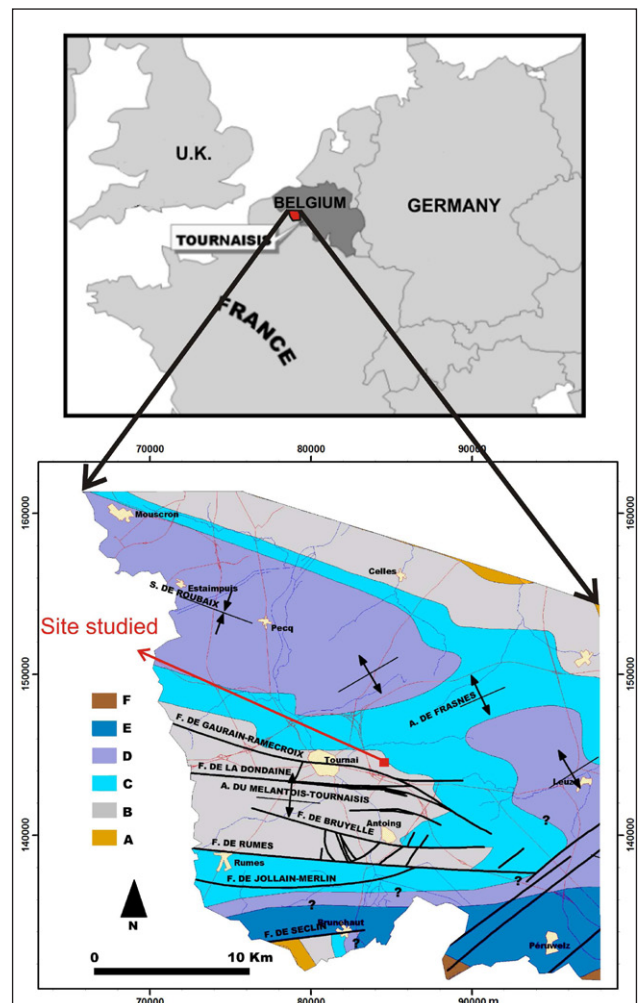

Figure 1: Location and structural map of the Tournaisis. A: sandstones, shales and shaly limestones of the Devonian formations, B: argilo-siliceous limestones of Tournai and Antoing formations (excluded Warchin Member), C: argilo-siliceous limestones of the Warchin Member of the Antoing formation, D: limestones of the Pecq formation (Visean), E: limestones from other Visean formations, F: Namurian formations. The geographical units are given in Belgian Lambert 72 plane coordinates.

Even if karst terrains remain a challenging context for geophysical investigations, continuous development of acquisition and processing techniques have significantly improved their imaging abilities. They are minimally intrusive and may prove cost-effective. These imaging techniques are therefore of increasing interest to improve the knowledge of underground conditions. However, it is sometimes difficult to select the appropriate technique among the wide range of geophysical methods available. Moreover, the results that could be expected are strongly dependent on the geological context. To help engineers dealing with karst management in the specific context of the Tournaisis area, we draw an overview of the potential and limits of geophysical methods in such covered palaeokarst context. First, we describe the geology and the specificities of palaeokarst features in the Tournaisis. Then, we examine the petrophysical properties of the alterite (ghost-rock) contained within these palaeokarsts. After that, we evidence the main advantages and major limitations of relevant geophysical methods in the context of the Tournaisis. Finally, we illustrate the results that could be expected on a field experiment and show how these results could be used to solve geological and geotechnical problems.

2. Geological settings

The Tournaisis area is located in the south-eastern part of Belgium near the France border (Fig. 1). In this region, the bedrock is mainly composed of argillaceous and siliceous Carboniferous limestone (Hennebert & Doremus, 1997) from the parautochthonous cover of the Brabant Massif (Mansy et al., 1999). This bedrock is overlain, in a non-uniform way, by a cover that mainly consists of Cretaceous marls and chalks and sandy or clayey Tertiary sediments. The thickness of this cover ranges from a few meters near the city of Tournai to more than 100 m in the NW. In the Tournaisis area, the bedrock is marked by East to West dextral wrench faults taking part in the Melantois - Tournaisis faulted anticline structure (Fig. 1) dated as tardi-varsican. Later movements also affect Mesozoic and Cenozoic sediments (Hennebert, 1998).

The Paleozoic bedrock altitudes are linked with the structure even if the relief is fairly flat in the area. According to Hennebert & Doremus (1997), the bedrock altitudes range between 30 and 40 meters a.s.l. near the anticline axis. Away from the anticline axis, the bedrock plunges towards the NW and the SW, consequently the cover thickness increases. Cretaceous marls and chalks are
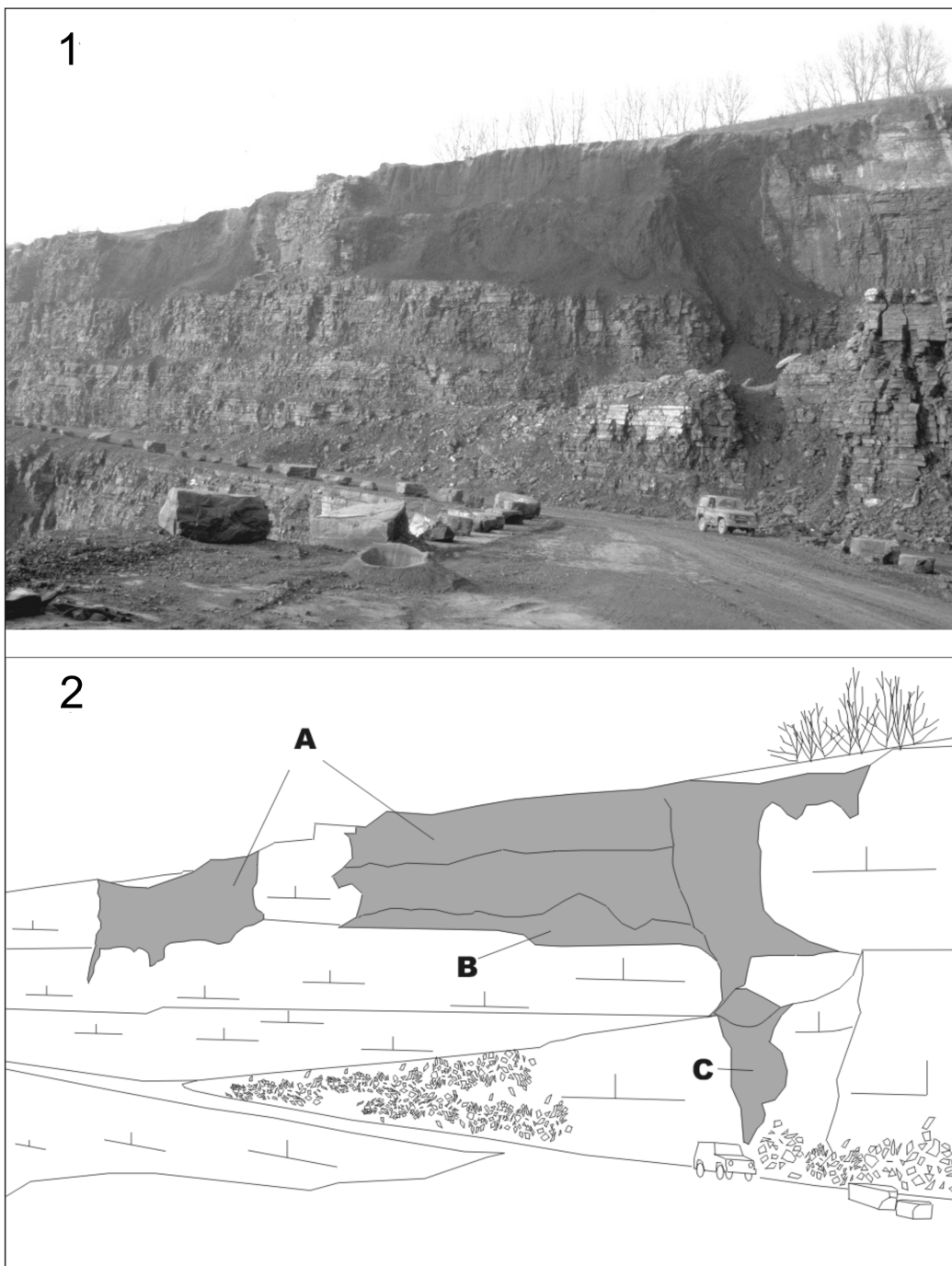
Figure 2: Photograph (1) and interpretative sketch (2) of a quarry face located near the "Rieu de Warchin" site showing typical weathered zones found in the Tournaisis (Kaufmann et al., 2012).
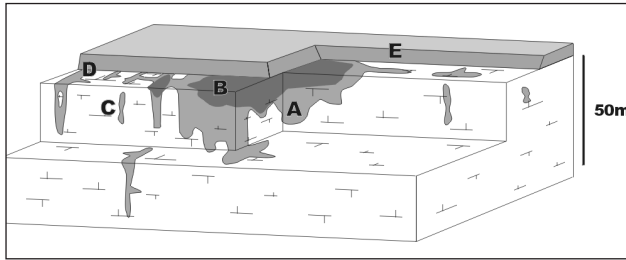
Figure 3: Synthesis of typical palaeokarstic features visible in the Tournaisis; A: a wide zone slot of weathering products; B: "cherts breccias" containing consolidated alterite at the top of wide slots; C: narrow slots; D: elongated slots also known as "weathered corridors"; E: cover materials (after Kaufmann, 2000).

mainly present in the western and southern parts of the Tournaisis area while Cenozoic sediments cover the whole area. The nature and thickness of the latter is mainly dependent on the actual relief which results of their erosion.

## 3. Palaeokarst and Ghost-rock properties

Even if the fairly flat relief of the Tournaisis area shows few landforms typical of karst terrains, quarry faces (Fig. 2) suggest that palaeokarst features are common in the underlying limestone (e.g., Quinif, 2010, Kaufmann et al., 2012). A synthesis of the different types of karst features found in limestone in the Tournaisis area is given on Fig. 3 (Kaufmann, 2000). These karst features formed prior to the deposit of the Tertiary sediments. Sinkholes occur when cover materials are washed away into the underlying bedrock voids.

3.1 Palaeokarst features

Karst features mostly develop in association with discontinuity planes (joints) by progressive dissolution of the carbonates. As dissolution processes occurred under low hydraulic gradient, a soft and porous weathering residue, called ghost-rock, often remains in place (Quinif, 2010). A typical result of the weathering processes is a profile with 1 to 10 m wide and 10 to 30 m high

slots (Sowers, 1996) (also called grikes or cutters elsewhere) between blocks of intact rock. The main specificity of this profile is that these slots mainly contain an isalterite (weathering product with slight or no change in rock volume and remnant rock structure), as defined by Delvigne (1998), except at their top. As the host limestone is siliceous, this isalterite is also siliceous, but a significant content of carbonate may remain in some of the intermediate weathering products. The porosity is commonly very high (up to 50% or more) as shown by Kaufmann et al. (1999), Quinif (2010), Kaufmann et al. (2012) and Dubois et al. (2014). In areas of intense weathering, palaeokarst features may interconnect leading to complex geometries of the weathered zones (Fig. 3). Due to the presence of the cover, no distinctive karst landforms are visible in the relief except for sinkholes that open up.

In the Tournaisis, most new sinkholes develop directly above these palaeokarst features (Kaufmann, 2000), mainly in areas of groundwater table lowering in the karst aquifer as shown by Kaufmann & Quinif (1999, 2002). As a consequence of dewatering, underground voids develop by isalterite compaction, collapse and transport. This process is speeded up where a perched aquifer discharges into the limestone aquifer. The cavity that is created grows and migrates upwards leading to a localized subsidence or collapse of the ground surface. Processes leading to the formation of such sinkholes are depicted on Fig. 4. Depending on the hydrogeological context, especially the presence of a perched aquifer in the cover, we propose two conceptual models to describe the successive steps of the formation of sinkholes in the Tournaisis area. In both cases, the precursor event is the lowering of the groundwater table in the limestone aquifer due to intensive pumping for water supply. In the absence of a perched aquifer (case 1), the isalterite progressively settles creating a small cavity (step A). Depending on the mechanical resistance of the isalterite and the cover materials, the top of this cavity successively falls down and the sinkhole progressively reaches the surface (steps B to D). When a perched aquifer is present in the cover materials (case 2), the process is similar until the sinkhole reaches the base of the perched aquifer (steps A and B). When the sinkhole reaches the perched aquifer, huge inputs of groundwater occurred when the perched aquifer discharges into the limestone aquifer. These inputs accelerate the migration of the sinkhole as
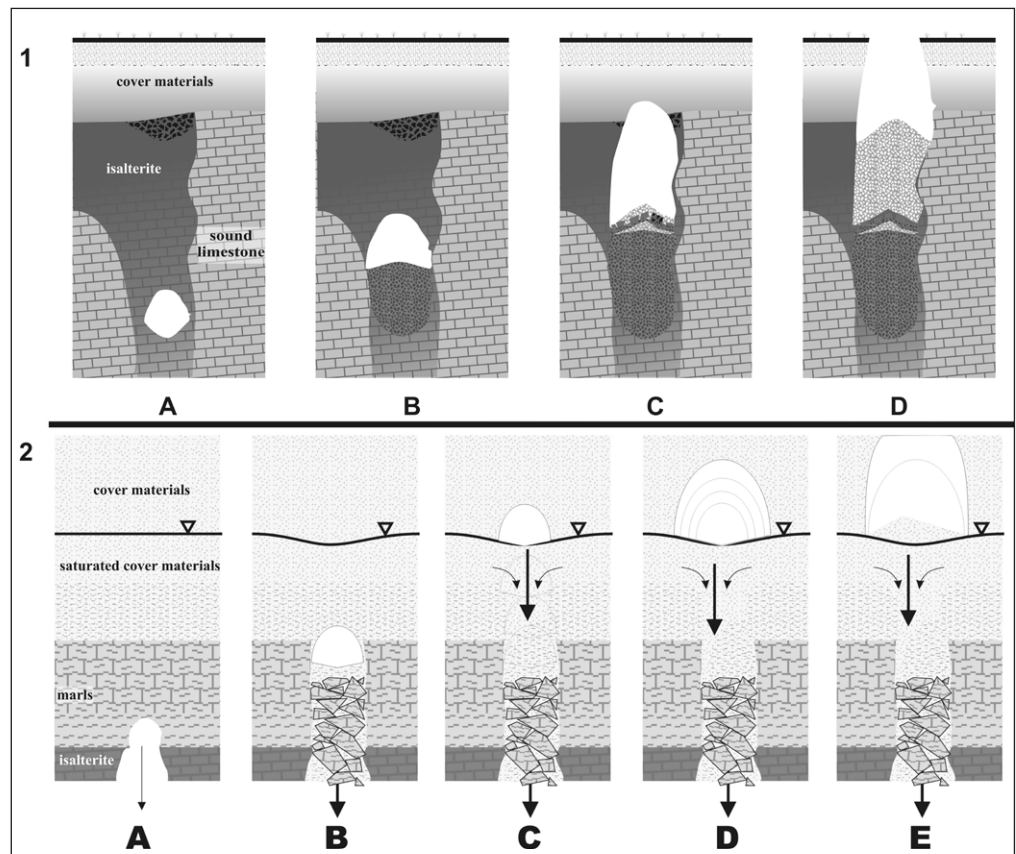
Figure 4: Successive steps (A, B, C, D, E) of the formation of a subsidence sinkhole in the Tournaisis when 1: cover materials did not contain an aquifer or 2: a perched aquifer is present inside cover materials (after Kaufmann, 2000).

the finer materials are washed away downwards. A cavity finally forms above the groundwater table (step C). The top of this cavity progressively falls down depending on the mechanical properties of the upper cover materials (step D) while the finer materials still being washed away down. Finally, the sinkhole reaches the surface (step E).

Though the Cretaceous cover could be viewed as a caprock, its mechanical properties are rather weak. Moreover, it is covered by at least several meters of poorly consolidated sediments. Thus sinkholes in the Tournaisis are regarded as subsidence sinkholes according to the sinkhole terminology used in Waltham et al. (2005). Subsidence sinkholes in the Tournaisis are circular or elliptical in plan and cylindrical or conical in profile while diameter and depth commonly range between 5 and 10 m. Larger sinkholes up to 50 m in diameter and 20 m in depth have been reported.

3.2 Ghost-rock petrophysical properties

We will focus on the characterization of the relevant ghost-rock petrophysical properties for their geophysical detection. Detailed observations and measurements conducted on quarry faces showed that strong variations in properties should be expected over short distances (Dubois et al., 2014). However, materials observed on quarry faces are already affected by dewatering and oxygenation. Petrophysical properties measured on these materials might not be fully representative of the in-situ conditions. However, in-situ properties are difficult to measure elsewhere as palaeokarst features must be located prior to measuring. To assess these in-situ properties, boreholes are required either for direct measurements when possible or for recovering undisturbed samples. As the consistency of ghost-rock is highly variable from firm and brittle to almost liquid, right sampling is also a challenging task. Available tests were

developed either for rock samples or for soils. Selecting testing devices and protocols thus remains difficult as isalterites range from rocky materials (zones II and III in Dubois et al., 2014) to loose soils (zones IV and V in Dubois et al., 2014). Measurements conducted in-situ or on undisturbed samples (Kaufmann et al., 1999 and Kaufmann, 2000) and those performed on quarry faces both showed that ghost-rock materials present a lower density (down to 4 times less (Dubois et al., 2014)), a higher porosity (up to 50 times more (Dubois et al., 2014)) and a higher permeability (up to 5 times more (Dubois et al., 2014)) than the surrounding bedrock. They also show a lower resistance to penetration when CPTs are conducted. A lower pressiometric modulus is also commonly measured in strongly weathered zones when using Ménard pressure-meter tests.

4. Mapping palaeokarst features through geophysical investigations: challenges and potentials

As stated in section 3, the main targets in the Tournaisis are slots containing saturated or nearly saturated ghost-rock rather than empty conduits or cavities. Often considered as a cavity detection problem before the last decade and tackled in this way, the detection and mapping strategies have since evolved as these phenomena are better understood and imaging techniques have improved. Given the field observations and the results of laboratory measurements described in section 3.2, strong variations in petrophysical properties, especially in density, porosity and permeability, are expected between isalterite, especially zones IV and V, and limestone. Since weathering processes lead to the development of a microporosity, the isalterite saturation ratio remains high even when dewatered due to soil suction and surface tension. This results in a lower contrast in bulk density than in dry density. It also leads to a significant increase in bulk electrical conductivity as it strongly depends on

Geophysical methods		Effects of enhanced (micro)porosity on properties	Main advantages	Major limitations
Microgravimetry		decrease in density	direct link with increase in porosity / macrovoids 2D/3D mapping	limited contrast in density due to high saturation ratio acquisition time and associated costs
ERT		increase in water content ⇨ decrease in resistivity	high contrast in resistivity 2D/3D imaging	resolution at depth sensitivity below conductive layers
EM Methods	**FDEM (Slingram)**	increase in water content ⇨ increase in conductivity	high contrast in conductivity 2D mapping	conductive layers near the surface ⇨ limited depth of investigation poor vertical resolution due to the limited frequency range covered by commercial devices
	TDEM	increase in water content ⇨ increase in conductivity	high contrast in conductivity 1D/2D imaging	highly sensitive to ambient EM noise ⇨ not recommended in urbanized areas
	VLF	increase in water content ⇨ increase in conductivity	easy and quick acquisition lateral resolution	reception of the appropriate radio transmitters (except for academic prototype equipment) poor vertical resolution (except for academic prototype equipment)
	GPR	increase in water content ⇨ decrease in resistivity and increase in dielectric permittivity	high lateral and vertical resolution 2D/3D imaging	conductive layers near the surface ⇨ strongly limited depth of investigation
Seismic methods	**Refraction**	decrease in density ⇨ decrease in V_P increase in Poisson's ratio ⇨ decrease in V_S	2D/3D imaging	moderate contrasts in relevant properties hidden-layer problems limited depth of investigation
	Reflection	decrease in density ⇨ decrease in V_P and in seismic impedance increase in Poisson's ratio ⇨ decrease in V_S	2D/3D imaging greater depths of investigation (lateral resolution at depth?)	<u>Work in progress</u> when cover thickness is limited, separating shallow reflections from shallow refractions may prove difficult, if not impossible
	Active Surface Waves	increase in Poisson's ratio ⇨ decrease in C_R	1D/2D imaging high signal to noise ratio	<u>Work in progress</u> lateral resolution (1D inversion) limited depth of investigation

Table 1: Main advantages and major limitations of effective geophysical methods when applied to the detection and mapping of palaeokarst features in cover-collapse context such as in the Tournaisis area.

the porosity, water saturation and electrical conductivity of the electrolyte (Archie, 1942). According to the empirical relationship proposed by Wyllie et al. (1956, 1958), P-waves velocities (V_p) of saturated elastic materials presenting a matrix velocity larger than the fluid velocity should decrease as the porosity increases. When considering unsaturated rocks, a more complex behaviour might be expected as V_p first decreases and then increases when the saturation increases (*e.g.* Duffaut & Homand, 2000). The Poisson's ratio of the isalterite should be larger than for sound limestone (*e.g.* Lavergne, 1986). As the ratio between P-waves velocities and S-waves velocities (V_s) increases with the increase in Poisson's ratio, S-waves velocities of ghost-rock are expected to be lower than for limestone. A similar trend is also expected for Rayleigh surface waves velocities (C_R).

These contrasts in petrophysical properties open doors to the geophysical detection of these weathered zones. In details, the possibility to detect them will depend especially on the target size, burial depth and properties of the cover materials. Mapping these targets is even more demanding than straightforward detection. It depends on the imaging capabilities of the selected techniques and devices, especially data quality, resolution, depth of investigation and sensitivity given the field conditions (ambient noise, accessibility, layout). Isolated slots containing ghost-rock can be viewed as 2.5D targets that could easily be imaged using appropriate profiling (1D layout orthogonal to the slot direction). However, when considering several slots aligned along different directions and crossing or connecting together, the targets exhibit complex 3D geometries that require at least 2D acquisition layouts. From a technical point of view, for imaging deeper targets cross-hole techniques are probably the best choice in terms of resolution (*e.g.,* Deceuster et al., 2006). However, a significant number of boreholes is required to reconstruct the 3D geometry of palaeokarst features in the investigated area. Therefore, cross-hole techniques will mainly be considered for the purpose of large projects of limited extent that cannot be easily relocated. These techniques would not be affordable for most of the other cases. Thus, for the latter, surface geophysical methods are an appealing alternative when the target depth is not too deep.

Given those facts, potentially effective geophysical methods include microgravimetry, electrical resistivity tomography (ERT), electromagnetic (EM) methods (including frequency domain (FDEM) methods at low induction numbers (Slingram), time domain (TDEM) methods, very low frequency (VLF) methods and ground penetration radar (GPR)) and a wide range of seismic methods. The main advantages and major limitations of these methods are summarized in Table 1. In the Tournaisis,

several attempts to map palaeokarst features were carried out using microgravimetry (*e.g.*, Michiels et al., 1985), FDEM (*e.g.*, Michiels et al., 1985), radiometric (*e.g.*, Vergari et al., 1995; Kaufmann, 2000) and ERT methods (*e.g.*, Quinif & Rorive, 1990; Vergari et al., 1995; Kaufmann & Quinif, 1999; Kaufmann et al., 2006, 2009, 2012). Microgravimetry intensive 2D surveys were in some cases able to locate wide palaeokarst slots under a 10 to 15 m thick unconsolidated overburden (e.g., Kaufmann et al., 2006). However, this type of survey is demanding and expensive. Therefore, they are mainly considered for the purpose of critical infrastructures directly threatened by sinkhole activity. Even if several authors (e.g., Bosch & Müller, 2005, Chalikakis, 2006, He et al., 2006, Valois et al., 2010) successfully apply EM methods to detect common karst features (*e.g.,* epikarst zone, air- or water-filled cavities, preferential pathways for ground water flow), these methods were no often successfully applied in the Tournaisis area. Since palaeokarst features are commonly covered by at least several meters of 50 to 100 mS/m conductive materials (clays, argillaceous silts or marls), some EM methods are strongly crippled. This is especially the case for the penetration depth of GPR which is limited to one or a few meters in such context. The penetration depth of FDEM methods thus ranges from a few meters to one or two tenths of meters. Currently, ERT methods remain the most effective while affordable detection and mapping techniques in most cases. Recent works exhibit the potential of seismic methods to supplement ERT (e.g., Chalikakis et al., 2011, Mari & Mendes, 2012, Valois et al., 2011) and expand the scope of geophysical detection of covered palaeokarst features.

5. Illustration

In this section, we illustrate our purpose. First, we show some results of ERT and seismic surveys applied to palaeokarst detection in the Tournaisis. These results are assessed using numerous geotechnical data and geological knowledge. Then, we show how these results could be used to solve geological and geotechnical problems.

5.1. Site description

This site is located about five hundred meters west from a limestone quarry near 'Rieu de Warchin' stream at Gaurain-Ramecroix. Water abstraction for quarry works locally increases the regional decline of the water table. Since 1984 many sinkholes (Fig. 5) opened up along the stream bed (Quinif et al., 1985, Quinif & Rorive, 1990, Van Rantergem et al., 1993, Kaufmann & Quinif, 1999, Kaufmann, 2000). Excavation works were

Figure 5: Location of the 2D ERT profiles inside the investigated area (contoured in grey) at "Rieu de Warchin" site. Recorded sinkholes are drawn with black spots. The area delineated with a black polygon is the one presented in Fig. 10.
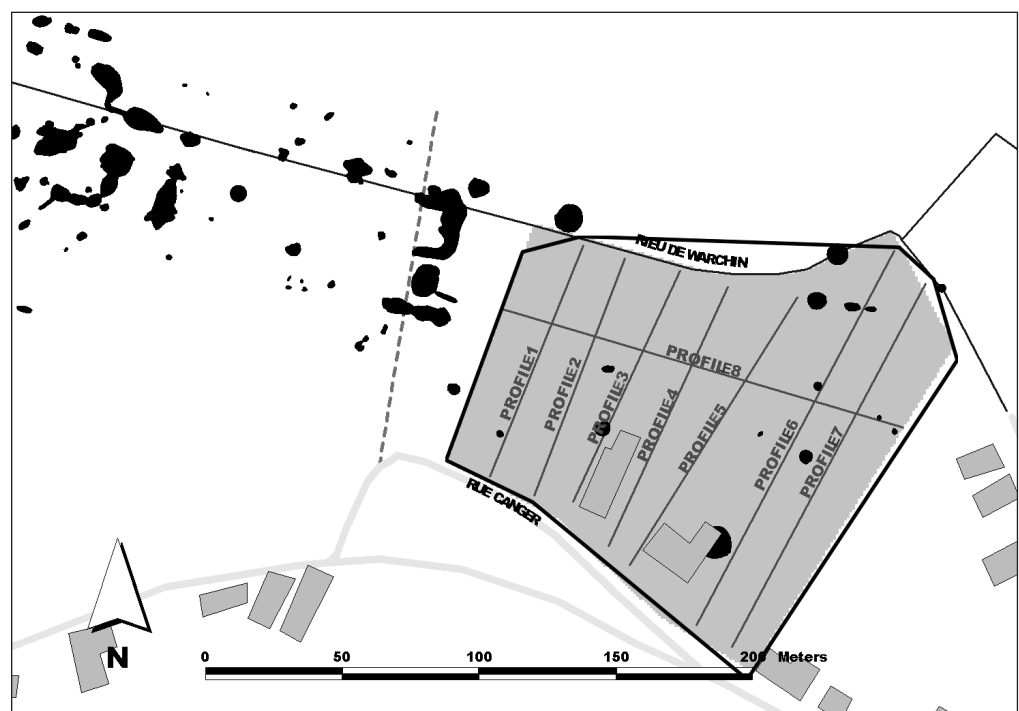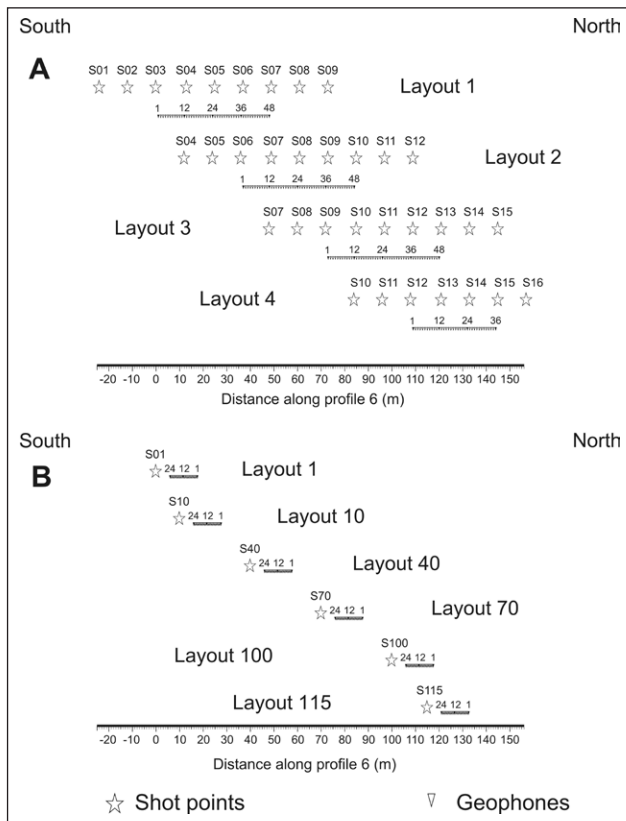
Figure 6: Layout spread patterns used for (A) seismic refraction survey and (B) shallow seismic survey along profile 6.

undertaken over and around sinkholes to precise the geological context. Depth to bedrock on this site is about 3 to 4 m and the cover mainly consists in silts and clayey sands. Excavations show that sinkholes occurred where the bedrock is highly weathered in 1 to 2 m wide slots oriented N105°E and N20°E. The slots directions are consistent with the main regional structure shown on Fig. 1.

5.2. Survey design

2D ERT measurements were conducted along 8 profiles of about 100 to 150 m in length (Fig. 5). Seven quasi-parallel profiles are oriented more or less N25°E. Spacing between these profiles is about 15 m. The last profile is oriented N105°E and crosses all the others. A 2.5 m electrode spacing was selected in order to reach a maximum depth of investigation of about 12 m with enough resolution to image slots. A combination of dipole-dipole (DD) and Wenner-Schlumberger (WS) arrays was used as Kaufmann & Quinif (2001) and Zhou et al. (2002) show that this combination of arrays gives the best results in a karst context. The inversion process was conducted within Res2DInv software (Loke, 2011) using the inversion parameters presented in Kaufmann et al. (2012).

Two shallow seismic surveys were also conducted along profile 6 (Fig. 5). The first one is a seismic refraction survey performed using a roll along technique using spreads composed of 48 4.5 Hz geophones with a 1-m spacing. The successive spreads have an overlap of 12 geophones. The source is an 8 kg

sledgehammer stroke on a thick aluminium plate. Sixteen shot stations were needed to complete the profile following the shot pattern described in Fig. 6A. This acquisition design allows the picking of the refracted waves even when the bedrock is deep as well as the detection of lateral variations in the first layer's velocities. The first arrivals were picked using Reflexw software and the inversion was carried out using a modified 2D SIRT algorithm (Kaufmann & Tshikala, 2011).

The second one consists in a shallow seismic reflection field experiment conducted to evaluate the potential of this method in supplementing common seismic refraction surveys. We use spreads composed of 24 4.5 Hz geophones with 50-cm spacing (Fig. 6B). A single shot station located 5 m to the South is used for every layout. The complete layout is then moved by 1 m northwards to survey the entire profile (115 layouts were needed to survey the entire profile). Thanks to this acquisition protocol, several common offset gather images can be drawn to image the seismic response of the subsoil. As this survey was our first attempt to image karst features with seismic reflection methods, further works are still needed to improve the acquisition and processing protocols.

5.3. Results

5.3.1. Electrical resistivity tomography (ERT)

Fig. 7 shows the results of the 2D ERT computed along profile number 6 (oriented S-N) as well as the results of the geotechnical investigations performed along this profile. From boreholes T09, T12 and T13 logs, three ranges in resistivities are associated to different lithologies: (1) < 50 Ω.m: corresponding to silts and clayey sands at the surface and to highly weathered limestone at depth; (2) resistivities between 50 and 250 Ω.m: corresponding to dryer residual soils, less weathered limestone at depth; (3) > 250 Ω.m: corresponding to competent bedrock. These resistivities are still low but are common on the argillaceous limestone of the Gaurain-Ramecroix formation (Kaufmann et al., 2012).

A continuous 3 to 4 m thick layer of low resistivities (< 50 Ω.m) is present at the surface (Fig. 7). These low resistivities correspond to cover materials mainly composed of silts and clayey sands. Below this layer the tomography shows intermediate to high resistivities at depth. The depth of the top of limestone ranges from 6 to 8 m in the southern part of the profile (between x-coordinates 0 and 80 m) and is around 4 m in the northern part as confirmed by CPTs and boreholes. Changes in resistivities are clearly pointed out inside limestone. Indeed, low to intermediate resistivities are found at bedrock depth in the first 80 m of the tomography. This indicates that the bedrock is more intensely weathered in the southern part of the profile. The lowest resistivities detected in depth are located where sinkholes S1 and S2 opened up. In the northern part, two main conductive anomalies are detected at depth. The first one is an 8 m thick vertical conductive anomaly (1) located at about 110 m along the X-axis below 4 m in depth. This anomaly is also located where a former sinkhole opened (S3). The second resistivity anomaly (2) is located in the most northern part of profile 6 (from 135 m along the X-axis to the end of the profile) and shows intermediate resistivities at bedrock depth (below 4 m). This slot is also confirmed by P20 and is consistent with the location of a former sinkhole (S4). As expected from ghost-rock petrophysical properties, weathered slots exhibits a conductive signature compared to the intact bedrock.
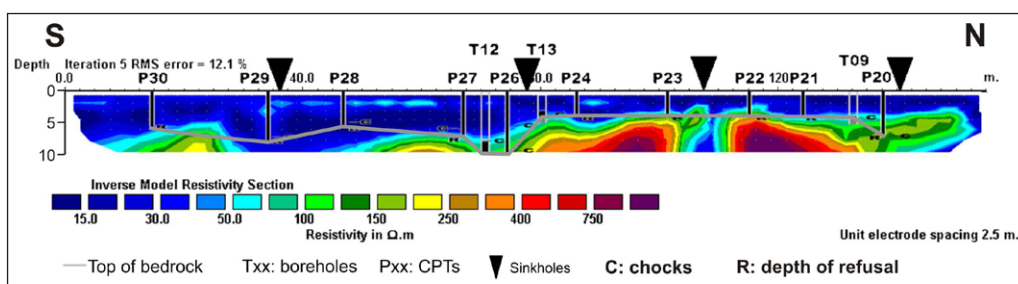
Figure 7: 2D resistivity tomography computed along profile 6. Pxx corresponds to static cone penetration tests and Txx indicates boreholes locations. The top of limestone bedrock (including slots containing ghost-rock) delineated with a grey line is estimated based on the results CPTs and boreholes.
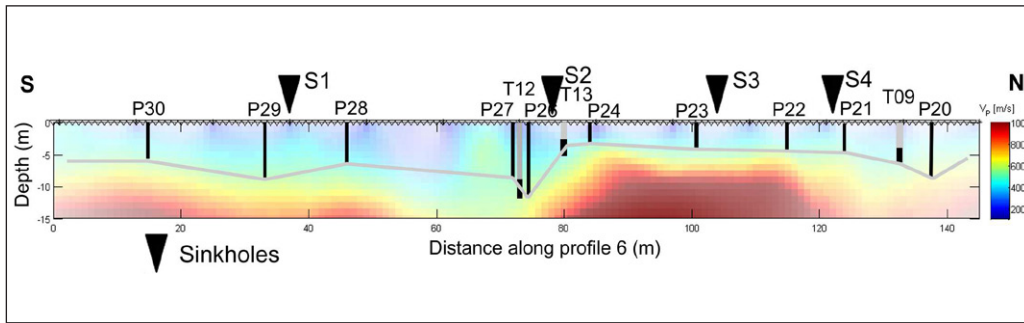
Figure 8: 2D seismic refraction tomography performed along profile 6. Pxx corresponds to static cone penetration tests and Txx indicates boreholes locations. The top of limestone bedrock (including slots containing ghost-rock) delineated with a grey line is estimated based on the results CPTs and boreholes.

These interpretations were conducted based on the comparison between ERT results and direct investigations (CPTS and boreholes). As those data are significantly consistent with each other, we did not appraise the image quality for this survey. When direct investigations are not available in sufficient number, several resolution indicators can be used to estimate the depth of investigation or to identify possible artefacts in the electrical structures. Among them, the most commonly used methods are based on the analysis of the model resolution matrix (e.g., Friedel, 2003, Hilbich et al., 2009, Oldenborger & Routh, 2009), the cumulative sensitivity matrix (e.g., Nguyen et al., 2009, Christiansen & Auken, 2012, Robert et al., 2012) and the DOI index (e.g., Oldenburg & Li, 1999, Marescot et al., 2003, Hilbich et al., 2009, Robert et al., 2011). Note that even if the RMS error seems significant, such high values can be attended in such contexts as we performed a 2D inversion while the karst geometry is strongly 3D. Lateral variations in resistivities therefore strongly influence the 2D reconstruction.

5.3.2. Seismic surveys

The results of the seismic refraction tomography performed along profile 6 (oriented S-N) are given in Fig. 8 as well as the results of the geotechnical investigations performed along this profile. Three ranges in P-wave velocities are also derived from boreholes T09, T12 and T13 logs: (1) < 200 m/s: corresponding to loose silts and clayey sands at the surface; (2) velocities between 400 and 650 m/s: corresponding to weathered limestone at depth; (3) > 650 m/s: corresponding to competent bedrock. Results similar to those found with ERT data can be obtained when interpreting the seismic tomography given in Fig. 8. The intermediate P-wave velocities (2) are found where the intermediate resistivity anomaly zones were evidenced. The general shape of the top of sound limestone is almost identical to the one derived from Fig. 7 and is also consistent with the CPTs and borehole data. The main difference is that no velocity anomaly is pointed out at depth at sinkhole S3 location. This is probably due to the limited width of the palaeokarst slot and to its vertical structure. Indeed, this kind of low velocity vertical structure is often poorly reconstructed by surface seismic refraction tomography imaging techniques, especially when its thickness is small compared to the geophone spacing. Moreover, P-waves directly crossed these thin weathered slots to gain high velocity zones (bedrock).

The unfiltered common offset gather image drawn using the 5 m offset from the shallow seismic survey shows diffraction hyperboles at S3 location (Fig. 9). These hyperboles are probably

linked with the vertical palaeokarst slot. Moreover, lateral variations identified in ERT and in seismic refraction tomography are also visible on this section. Indeed, in the northern part of the profile (after 75 m along the X-axis), the reflected waves exhibits a smooth shape and a regular recurrence except where hyperboles are present. This may be the signature of the sound limestone bedrock located at a limited depth. In the southern part of the profile (from 0 to 75 m along the X-axis), the reflected waves exhibit a more scattered shape and a stronger attenuation with time. These are probably linked to the changes in petrophysical and mechanical properties in the ghost-rock. However, further works are still needed to ensure of these interpretations.

5.4 Effective ERT investigation strategy to solve engineering geology problems

Site-specific ERT based investigation strategy can be designed to help engineers dealing with the design of construction projects in such karst context. On this site, eight 2D ERT profiles have been conducted as well as 46 CPTs and 16 boreholes. A 3D resistivity model was computed based on the inverted resistivities (Kaufmann et al., 2012). Vertical resistivity profiles were then computed at each CPT location in order to establish a resistivity law to discriminate between sound limestone and weathered rock. This empirical law is probably site-specific and mainly depends on the geological context and the type of electrical resistivity imaging performed (1D, 2D, 3D, cross-borehole). Comparing resistivities of the model blocks to this empirical law finally allows the computation of a 3D depth to bedrock model. This methodology is fully detailed in Kaufmann et al. (2012).

Two classical engineering problems are considered to illustrate how this depth to bedrock model could be used by engineers dealing with the design of site-scaled projects. The first one (case 1) is the deep foundations of buildings (e.g., pile foundations). The second engineering problem examined (case 2) is the horizontal sinking of pipes (e.g., sewer pipes, high-pressure pipelines, gas pipes). These two engineering problems are tested on two hypotheses: (Hyp. A) sound bedrock is present at a depth smaller than 10 m; (Hyp. B) bedrock is weathered at least on its first 2 m below 3.5 m depth (below loose soils). In order to compare the reliability of the two methods of investigations, performance tests based on borehole data (ground truth) were conducted on the depth to bedrock models computed from CPT data and from the 3D resistivity model by means of contingency tables analysis (Kaufmann et al., 2012). Given the different depth

Figure 9: Common offset gather seismic image computed using a 5-m offset along profile 6 (unmuted traces) showing diffraction hyperboles at sinkhole S3 location (110 m along the X-axis).
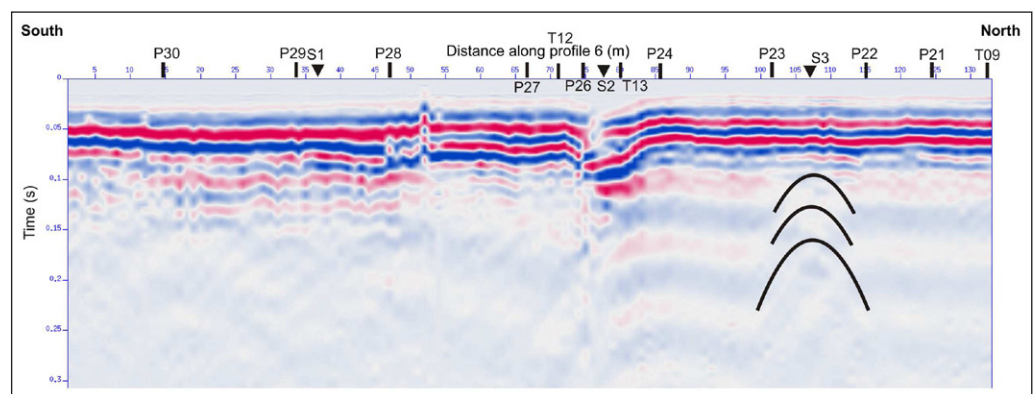
to bedrock models, Fig. 10 shows maps of areas suitable or not for conducting works in both hypotheses. For Hyp. A, areas suitable for pile foundations are drawn in pink. When considering CPT only (Fig. 10A), the entire area is classified as suitable. However, performance test showed that the CPT depth to bedrock model is unreliable in this case. This evidences the need for other detection strategies. When considering ERT data (Fig. 10C), only the northern part of the investigated zone is suitable for deep foundation of buildings. This model was proved to be highly reliable based on performance tests. For Hyp. B (Fig. 10B and Fig. 10D), both depths to bedrock models were found at least reliable to detect suitable areas and provide almost similar results: the northern part of the area (drawn in pink) is unsuitable for the horizontal sinking of pipe.

These examples show that a site-specific ERT based investigation strategy can, at least significantly, discriminate between sound rock and palaeokarst features for both case studied while this is not always true for the depth to bedrock model computed from CPTs data. Based on these results, we recommend to conduct ERT investigations coupled with several CPTs located based on the results of the geophysical investigations when dealing with site-scaled projects in areas with medium or high karst constraint in the Tournaisis area. Indeed, CPTs are needed in both areas (where sound rock is present and where karst features are located) in order to compute the experimental resistivity law.

According to Zhou et al. (2002) and Kaufmann & Quinif (2001), a combination of dipole-dipole and WS arrays is recommended for the ERT data acquisition in karst context. When the depth of investigation needed is limited to a few decades of meters, 3D ERT surveys should be preferred to 2D ERT, in particular in areas where the main directions of fracture are unknown. When the depth to bedrock increases, 2D ERT surveys could be acquired along several parallel profiles (preferably perpendiculars to the main direction of fracture) and inverted together using a 3D inversion routine to improve the reconstruction of the 3D geometry of such karst features. When surface measurements cannot be performed (e.g., limited space available in urbanized areas, existing buildings or infrastructures above the targets), cross-hole ERT surveys may be conducted to detect karst features and improve the resolution at depth (e.g., Deceuster et al., 2006, Leontarakis & Apostolopoulos, 2013).

Based on the results of the seismic refraction tomography shown on Fig. 8, it sounds interesting to compute a depth to bedrock model based on a 3D velocity model obtained using a similar approach even if acquiring appropriate dataset and processing them is more demanding than with ERT. This alternative approach should therefore be justified when the ERT based strategy failed due to adverse site conditions. In some cases, it could prove valuable to combine ERT and seismic interpretations to compute a depth to bedrock model. However, further works are still needed to completely assess the efficiency of the seismic refraction method in solving engineering problems in such karst context.

## 6. Conclusions and perspectives

In the Tournaisis area, palaeokarst features mainly exhibit an alternated pattern of pinnacles and slots which contain a soft weathering residue called ghost-rock. We presented the key characteristics of these palaeokarst features. We discussed the main contrasts in petrophysical properties that can be expected between ghost-rock and bedrock. We evidenced the main advantages and major limitations of potentially effective geophysical investigation methods: microgravimetry, EM methods, ERT and seismic methods. Among these methods, ERT remains the most effective while affordable detection and mapping technique in most cases. As recent works exhibited the potential of seismic methods to supplement ERT in karst contexts, we focused on the application of these two methods. To illustrate our purpose, we described some results of ERT and seismic surveys applied to palaeokarst detection on a well-documented site. These results are assessed using numerous geotechnical data and geological knowledge. Using a site-adapted ERT based investigation strategy, reliable decision maps relative to two different civil engineering problems were designed. As seismic refraction tomography also showed relevant results, a similar strategy could be derived from seismic refraction tomographies. Other shallow seismic experiments should be further investigated as common offset gather images seem to supplement the interpretation of seismic refraction imaging. However, data acquisition and processing in seismic surveys would be more demanding than for ERT.

8. References

Andreo, B., Ravbar, N. & Vias, J.M., 2009. Source vulnerability mapping in carbonate (karst) aquifers by extension of the COP method: application to pilot sites. Hydrogeology Journal, 17, 749–758.

Archie, G.E., 1942. The electrical resistivity log as an aid in determining some reservoir characteristics. Petroleum Transactions of AIME, 146, 54–62.

Benson, R.C., Yuhr, L. & Kaufmann, R.D., 2003. Assessing the risk of karst subsidence and collapse. American Society Civil Engineers Geotechnical Special Publication, 122, 31-39.

Bosch, F.P. & Müller, I., 2005. Improved karst exploration by VLF-EM gradient survey: comparison with other geophysical methods. Near Surface Geophysics, 3, 299–310.
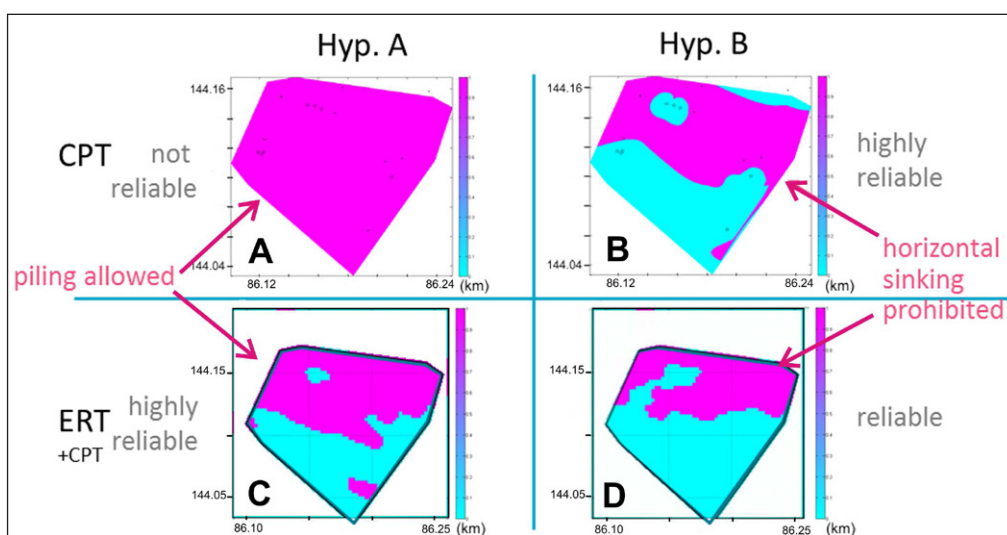
Figure 10: Decision maps designed for the considered engineering problems in the area drawn in grey on Fig. 5. Areas depicted in pink are suitable for building on pile foundations (Hyp. A) and unsuitable for horizontal sinking of pipes between 3 and 5 m in depth (Hyp. B). Maps A and B are drawn from CPTs depth to bedrock model only while maps C and D are drawn using CPTs and the 3D resistivity model computed from the eight 2D profiles of Fig. 5. The geographical units are given in Belgian Lambert 72 plane coordinates.

Caramanna, G., Ciotoli, G. & Nisio, S., 2008. A review of natural sinkhole phenomena in Italian plain areas. Natural Hazards, 45, 145–172.

Chalikakis, K., 2006. Application de méthodes géophysiques pour la reconnaissance et la protection des ressources en eau dans les milieux karstiques [Geophysical methods applied to water exploration and protection in karst environment]. PhD Thesis, Université Pierre et Marie Curie-Paris 6, France, 217 p.

Chalikakis, K., Plagnes, V., Guérin, R., Valois, R. & Bosch, F.P., 2011. Contribution of geophysical methods for karst system exploration. An overview. Hydrogeology Journal, 19, 1169-1180.

Christiansen, A.V. & Auken, E., 2012. A global measure for depth of investigation. Geophysics, 77 (4), WB171–WB177.

Cooper, A.H., 2008. The GIS approach to evaporite-karst geohazards in Great Britain. Environmental Geology, 53, 981–992.

Davis, A.D., Long, A.J. & Wireman, M., 2002. KARSTIC: a sensitive method for carbonate aquifers in karst terrain. Environmental Geology, 42, 65–72.

Deceuster, J., Delgranche, J. & Kaufmann, O., 2006. 2-D cross-borehole resistivity tomographies below foundations as a tool to design proper remedial actions in covered karst. Journal of Applied Geophysics, 60, 68-86.

Delvigne, J.E., 1998. Atlas of micromorphology of mineral alteration and weathering. The Canadian Mineralogist, Special Publication, ORSTOM Editions, France, 494 p.

Dörfliger, N., Jeannin, P.Y. & Zwahlen, F., 1999. Water vulnerability assessment in karst environments: a new method of defining protection areas using a multi-attribute approach and GIS tools (EPIK method). Environmental Geology, 39(2), 165–176.

Dubois, C., Quinif, Y., Baele, J.M., Dagrain, F., Deceuster, J. & Kaufmann, O., 2014. Mineralogical and petrophysical properties evolution of a weathered limestone in southern Belgium. Geologica Belgica, 17, 1-8.

Duffaut P. & Homand F., 2000. Manuel de mécanique des roches. Tome 1 : fondements. Presse des Mines, Paris, France, 280 p.

Edmonds, C.N., Green, C.P. & Higginbottom, I.E., 1987. Subsidence hazard prediction for limestone terrains. Bulletin Association Engineering Geologists, 3, 15-25.

Friedel, S., 2003. Resolution, stability and efficiency of resistivity tomography estimated from a generalized inverse approach. Geophysical Journal International, 153, 305-316.

Galve, J.P., Gutiérrez, F., Remondo, J., Bonachea, J., Lucha, P. & Cendrero, A., 2009. Evaluating and comparing methods of sinkhole susceptibility mapping in the Ebro Valley evaporite karst (NE Spain). Geomorphology, 111, 160–172.

Goldscheider, N., 2005. Karst groundwater vulnerability mapping: application of a new method in the Swabian Alb, Germany. Hydrogeology Journal, 13, 555–564.

He, L., Feng, M., He, Z. & Wang, X., 2006. Application of EM methods for the investigation of Qiyueshan tunnel, China. J Environ Eng Geophys, 11, 151–156.

Hennebert, M. & Doremus, P., 1997. Notice explicative de la Carte Gégologique de Wallonie (1/25.000) – Planche 37/5-6 Hertain-Tournai. Ministère de la Région Wallonne, 63 p.

Hennebert, M., 1998. L'anticlinal faillé du Mélantois-Tournaisis fait partie d'une « structure en fleur positive » tardi-varisque. Ann. Soc. Géol. du Nord, 6 (2), 65-78.

Hilbich, C., Marescot, L., Hauck, C., Loke, M.H. & Mäusbacher, R., 2009. Applicability of electrical resistivity tomography monitoring to coarse blocky and ice-rich permafrost landforms. Permafrost and Periglacial Processes, 20, 269–284.

Kaufmann, O. & Quinif, Y., 1999. Cover-collapse sinkholes in the "Tournaisis" area, southern Belgium. Engineering Geology, 52, 15-22.

Kaufmann, O. & Quinif, Y., 2001. An application of cone penetration tests and combined array 2D electrical resistivity tomography to delineate cover-collapse sinkholes prone areas. In: Beck, B.F. & Herring, J.G. (eds), Geotechnical and Environmental Applications of Karst Geology and Hydrology, 359-364. Balkema: Lisse.

Kaufmann, O. & Quinif, Y., 2002. Geohazard map of cover-collapse sinkholes in the Tournaisis area, southern Belgium. Engineering Geology, 65, 117-124.

Kaufmann, O. & Tshikala, F., 2011. Parallelized 2D fresnel volumes traveltime tomography. In Marschallinger, R. & Zobl, F. IAMG 2011 Salzburg proceedings, 594-601.

Kaufmann, O., 2000. Les effondrements karstiques du Tournaisis : genèse, évolution, localisation, prévention. Speleochronos, Hors-Série, 350 p.

Kaufmann, O., Bini, A., Tognini, P. & Quinif, Y., 1999. Etude microscopique d'une altérite de type fantôme de roche. Karst 99 European Conference, France, 129-133.

Kaufmann, O., Deceuster, J. & Quinif, Y., 2012. An electrical resistivity imaging-based strategy to enable site-scaled planning over covered palaeokarst features in the Tournaisis area (Belgium). Engineering Geology, 133-134, 49-65.

Kaufmann, O., Delgranche, J. & Deceuster, J., 2006. Geophysics for physical planning over covered karstic areas in the Walloon region of Belgium. SAGEEP 2006 Extended Abstracts, Environmental and Engineering Geophysical Society, Colorado (USA), 9 p.

Kaufmann, O., Lizin, P., Martin, T. & Deceuster, J., 2009. The role of geophysical investigations in physical planning over covered karstic areas in southern Belgium. Proceedings of Near Surface 2009, European Association of Geoscientists & Engineers, Dublin (Ireland), 4 p.

Kavouri, K., Plagnes, V., Tremoulet, J., Dörfliger, N., Rejiba, F. & Marchet, P., 2011. PaPRIKa: a method for estimating karst resource and source vulnerability—application to the Ouysse karst system (southwest France). Hydrogeology Journal, 19 (2), 339-353.

Lavergne, M., 1986. Méthodes sismiques. Editions Technip, Paris, 207 p.

Leontarakis, K. & Apostolopoulos, G.V., 2013. Model Stacking (MOST) technique applied in cross-hole ERT field data for the detection of Thessaloniki ancient walls' depth. Journal of Applied Geophysics, 93, 101-113.

Loke, M.H., 2011. Tutorial: 2-D and 3-D electrical imaging surveys. Revision 30th December 2011. 150 p., http://www.geoelectrical.com

Malik, P. & Svasta, J., 1999. REKS: an alternative method of Karst groundwater vulnerability estimation. Hydrogeology and Land Use Management, Proceeding of the XXIX Congress of the International Association of Hydrogeologists, Bratislava, Slovakia, 79–85.

Mansy, J.L., Everaerts, M. & De Vos, W., 1999. Structural analysis of the adjacent Acadian and Variscan fold belts in Belgium and northern France from geophysical and geological evidence. Tectonophysics, 309, 99-116.

Marescot, L., Loke, M.H., Chapellier, D., Delaloye, R., Lambiel, C. & Reynard, E., 2003. Assessing reliability of 2D resistivity imaging in mountain permafrost studies using the Depth Of Investigation index method. Near Surface Geophysics, 1, 57-67.

Mari, J.-L. & Mendes, M., 2012. High resolution 3D near surface imaging of fracture corridors and cavities by combining Plus-Minus method and refraction tomography. Near Surface Geophysics, 10 (3), 185-195.

Michiels, T., Schroeder, C. & Monjoie, A., 1985. Rapport de prospection géophysique à Gaurain-Ramecroix, Rieu de Warchin. Université de Liège, Faculté des Sciences Appliquées, Laboratoires de Géologie de l'Ingénieur et d'Hydrogéologie, Unpublished, 11 p.

Nguyen, F., Kemna, A., Antonsson, A., Engesgaard, P., Kuras, O., Ogilvy, R., Gisbert, J., Jorreto, S. & Pulido-Bosch, A., 2009. Characterization of seawater intrusion using 2D electrical imaging. Near Surface Geophysics, 7, 377-390.

Oldenborger, G.A. & Routh, P.S., 2009. The point-spread function measure of resolution for the 3-D electrical resistivity experiment. Geophysical Journal International, 176, 405-414.

Oldenburg, D.W. & Li, Y., 1999. Estimating depth of investigation in dc resistivity and IP surveys. Geophysics, 64, 403-416.

Pételet-Giraud, E., Dörfliger, N. & Crochet, P., 2000. RISKE: méthode d'évaluation multicritère de la vulnérabilité des aquifères karstiques. Application aux systèmes des Fontanilles et Cent-Fonts (Hérault, Sud de la France). Hydrogéologie, 4, 71–88.

Quinif, Y. & Rorive, A., 1990. Nouvelles données sur le karst du Tournaisis. Bull. Soc. Belge de Géol., 99 (3-4), 361-372.

Quinif, Y., 2010. Fantômes de roche et fantômisation - Essai sur un nouveau paradigme en karstogenèse. Karstologia Mémoires, 18, 196 p.

Quinif, Y., Bouko, Ph., Cantallina, R., Drumel, P. & Rorive, A., 1985. Découverte d'un réseau karstique superficiel à Gaurain-Ramecroix (Hainaut occidental, Belgique) à la faveur de nouveaux puits naturels. Bull. Soc. Belge de Géol., 94 (1), 45-50.

Robert, T., Caterina, D., Deceuster, J., Kaufmann, O. & Nguyen, F., 2012. A salt tracer test monitored with surface ERT to detect preferential flow and transport paths in fractured/karstified limestones. Geophysics, 77 (2), B55-B67.

Robert, T., Dassargues, A., Brouyère, S., Kaufmann, O., Hallet, V. & Nguyen, F., 2011. Assessing the contribution of electrical resistivity tomography (ERT) and self-potential (SP) methods for a water well drilling program in fractured/karstified limestones. Journal of Applied Geophysics, 75 (1), 42-53.

Sowers, G.F., 1996. Building on sinkholes: design and construction of foundations in karst terrain. ASCE Press, 202 p.

Thomas, B. & Roth, M.S., 1999. Evaluation of site characterization methods for sinkholes in Pennsylvania and New Jersey. Engineering Geology, 52, 147-152.

Valois, R., Bermejo, L., Guérin, R., Hinguant, S., Pigeaud, R. & Rodet, J., 2010. Karstic morphologies identified with geophysics around Saulges caves (Mayenne, France). Archaeological Prospection, 17, 151–160.

Valois, R., Camerlynck, C., Dhemaied, A., Guérin, R., Hovhannissian, G., Plagnes, V., Rejiba, F. & Robain, H., 2011. Assessment of doline geometry using geophysics on the Quercy plateau karst (South France). Earth Surface Processes and Landforms, 36, 1183-1192.

Van Dijck, F. & Michel, R., 2006. Les risques naturels en Région Wallonne. Karst and Physical Planning International Colloquium, Namur, Belgium, 93-109.

Van Rantergem, G., Bouckaert, P. & Quinif, Y., 1993. Une nouvelle grotte à Gaurain-Ramecroix. Bull. Soc. Belge Géol., 102 (3-4), 395-399.

Vergari, A., Quinif, Y. & Charlet, J.M., 1995. Paleokarstic features in the Belgian carboniferous limestones - implications to engineering. Karst geohazards: engineering and environmental problems in karst terrane. Proc. 5th conference, Gatlinburg 1995, 481-486.

Waltham, T., Bell, F. & Culshaw, M., 2005. Sinkholes and subsidence – Karst and Cavernous Rocks in engineering and Construction. Proxis, Chichester U.K., 382 p.

Wyllie, M.R., Gregory, A.R. & Gardner, G.H.F., 1956. Elastic wave velocities in heterogeneous and porous media. Geophysics, 21, 41-70.

Wyllie, M.R., Gregory, A.R. & Gardner, G.H.F., 1958. An experimental investigation of factors affecting elastic wave velocities in porous media. Geophysics, 23, 459-493.

Zhou W., Beck B.F. & Adams A.L., 2002. Effective electrode array in mapping karst hazards in electrical resistivity tomography. Environmental Geology, 42, 922-928.